Received May 5, 2022, accepted May 17, 2022, date of publication May 18, 2022, date of current version May 24, 2022.

Digital Object Identifier 10.1109/ACCESS.2022.3176452

Resonant Frequency Separation Characteristics of the Same-Order Hermite-Gaussian Mode in the Astigmatic Triangular Cavity of a Cavity Ring-Down Spectroscope

YIJIE REN[1,2], CHANGXIANG YAN[1,3], CONGJUN WU[1], SHAOMAN SONG[4], AND JING YUAN[1]

[1]Changchun Institute of Optics, Fine Mechanics and Physics, Chinese Academy of Sciences, Changchun 130033, China
[2]College of Materials Science and Opto-Electronic Technology, University of Chinese Academy of Sciences, Beijing 100049, China
[3]Center of Materials Science and Optoelectronics Engineering, University of Chinese Academy of Science, Beijing 100049, China
[4]Ji Hua Laboratory, Foshan 528200, China

Corresponding author: Congjun Wu (wucongjun789@163.com)

This work was supported in part by the National Natural Science Foundation of China (NSFC) under Grant 61805235, Grant 61905241, and Grant 61875192.

ABSTRACT Triangular planar ring resonant cavities are widely used in cavity ring-down spectroscopes (CRDS) because of the unique optical path advantage. Hermite-Gaussian theory is the classical method used to describe the beam in the resonant cavity. Since this theory can express the transverse electromagnetic mode (TEM) in the meridian plane and sagittal surface separately in an astigmatic triangular cavity, it has a unique advantage in the analysis of triangular cavities. However, among the many analyses of triangular ring-down cavities, existing theories of Hermite-Gaussian modes have not been able to reasonably explain the many phenomena observed in alignment and ring-down experiments. In this paper, the mechanisms of the effects of first-order Hermite-Gaussian mode on mounting alignment in CRDS instruments are investigated in depth. The frequency separation characteristics of the lower-order mode in the triangular cavity are verified in the mounting alignment stage. The separation characteristics of first-order mode can guide the misalignment of the two orthogonal planes separately. The resonant frequency separation property of the Hermite-Gaussian mode in a triangular ring-down cavity can also be applied to more complex odd-numbered cavity mirror resonant systems.

INDEX TERMS CRDS, Hermite-Gaussian mode, misalignment, triangular cavity.

I. INTRODUCTION

Use of the cavity ring-down spectroscopy (CRDS) technique has grown rapidly in recent years. It can rapidly measure various environmental trace gases and has a wide range of applications in the ground environment, space, and deep-sea fields [1]–[4]. It is currently also used in a wide range of applications in the biomedical and nuclear physics field [5]–[9]. Its core components are an external source laser and a resonant cavity, the coupling of which directly determines its detection accuracy.

The mounting alignment of the triangular resonant cavity has been widely analyzed in mode cleaner applications for gravitational wave detection, laser gyroscopes. Existing analytical methods include generalized ray matrix analysis based on perturbation theory [10]–[12]. However, analysis based on Hermit-Gaussian (HGs) theory can explain many of the phenomena in resonant cavities more rationally. Most analyses based on HGs theory are based on the fundamental mode [13]–[15]. In this paper, HGs modes refer to modes other than the fundamental mode. Most studies on HGs modes are based on systems with even numbers of cavity mirrors [16]–[18]. Studies of HGs modes are limited to analyses of mounting alignments. Fewer studies have been carried out on triangular cavities than straight cavities. In terms of the connection between a triangular ring cavity structure and the fundamental mode, Skettrup investigated the astigmatic properties of the triangular cavity [19], while Song investigated

The associate editor coordinating the review of this manuscript and approving it for publication was Baozhen Yao.

the effect of misalignment on the transmission efficiency of the fundamental mode in triangular cavities with different structures [20].

Theoretical studies on the approximation of HGs functions for lasers can be summarized into three categories based on 1) fundamental mode (TEM_{00}), 2) low-order mode (first- and second-order mode are dominant) affects the mounting alignment, and 3) high-order mode ($>20^{th}$ order, TEMmn, m+n>20) affect the ring-down characteristics. Most existing studies are limited to the analysis of the characteristics of fundamental mode, such as their transmission power, coupling coefficients, and beam waists [13]–[15]. Much of the research on lower-order mode in HGs theory is limited to the mounting aspect. For example, Sayeh summarized the excitation of HGs mode of various orders for an optical resonator with an external source [16]. Anderson demonstrated that misalignment and mismatch in a straight cavity induce coupling of off-axis mode [17]. Sampas added phase-modulated sidebands to indicate the extent of misalignment [18]. Many of the above studies are based on straight or four-mirror cavity resonators. The studies on triangular resonant cavities are also based on fundamental mode [19]–[20].

The theory and design of fundamental mode in various types of cavities have been well studied, and the low-order and high-order mode in straight cavities have been considered. However, the excitation of HGs mode in triangular ring-down cavities has not been studied systematically. The mechanisms of the different effects of HGs and fundamental mode in a triangular ring-down cavity during mounting alignment have not been systematically verified by CRDS experiments. Is the excitation of low-order modes only related to misalignment? Does the excitation of HGs model assist in eliminating mismatches and misalignments? Is the alignment method of the triangular cavity different from that of the straight cavity? This article provides an in-depth systematic study of the HGs mode of triangular cavities. This refines the theory of HGs mode in ring-down cavities.

This paper studies HGs mode in terms of a combination of the characteristics of a narrow linewidth light source and a high-reflectivity cavity in a CRDS system. The frequency distribution and amplitude excitation characteristics of each order of the HGs mode in the triangular ring-down cavity (except the fundamental mode) are systematically analyzed. First, it is theoretically concluded that the CRDS system causes strong suppression of the transmission of HGs mode. It is found that the resonant frequencies of same-order HGs mode in the meridian plane (y-z plane) and sagittal surface (x-z plane) are different. This is called the same-order mode frequency separation property of the triangular cavity. The frequency separation characteristics of HGs mode were experimentally verified step by step in the mounting alignment stage. Therefore, this paper investigates the frequency separation characteristics of the HGs mode in a triangular ring-down cavity. The theoretical understanding of the HGs mode in ring-down cavities is thereby improved. This provides a basis for improving the alignment and detection accuracy of a CRDS system based on a triangular cavity.

This paper focuses on the analysis of the lower-order in the HGs mode. In Section 2, the resonant frequency separation characteristics of HGs mode in triangular cavities are analyzed and compared with those in straight cavities. In Section 3, the transmission and excitation characteristics of the HGs mode in the triangular cavity are analyzed. In Section 4, alignment experiments show that the frequency separation characteristics of the HGs mode can guide the alignment of two orthogonal planes in a high-finesse triangular cavity. The conclusion is given in Section 5.

II. RESONANT FREQUENCY SEPARATION CHARACTERISTICS OF THE SAME-ORDER HERMITE-GAUSSIAN MODE IN THE TRIANGULAR CAVITY

The laser transverse field distribution $E(x,y)$ at a given propagation position $z(j)$ in the jth segment is described as a superposition of modes of the Gauss-Hermite basis u_{mn} [21],

$$E\left(x, y, z(j)\right) = E_0 \sum_{m,n} a_{mn} u_{mn}\left(x, y, q\left(z_{(j)}\right)\right) \tag{1}$$

where amn represents the complex amplitude of u_{mn} at the position $z(j)$. The complete form of u_{mn} is as follows:

$$\begin{aligned} &u_{mn}\left(x, y, q\left(z_{(j)}\right)\right) \\ &= H_m\left(\frac{\sqrt{2}}{\omega_{(q(z_{(j)}))}} x\right) H_n\left(\frac{\sqrt{2}}{\omega_{(q(z_{(j)}))}} y\right) \cdot \left(\frac{\omega_0}{\omega_{(q(z_{(j)}))}}\right) \\ &\quad \cdot \exp\left(-i\left(m+\frac{1}{2}\right)\phi_m\left(q\left(z_{(j)}\right)\right) - \frac{x^2}{\omega^2_{(q(z_{(j)}))}}\right) \\ &\quad \cdot \exp\left(-i\left(n+\frac{1}{2}\right)\phi_n\left(q\left(z_{(j)}\right)\right) - \frac{y^2}{\omega^2_{(q(z_{(j)}))}}\right) \end{aligned} \tag{2}$$

u_{mn} denotes the resonator eigenmode of order m, n in the jth segment, $q(j)$ is the complex beam parameter in the jth segment. u_{oo} represents the fundamental mode. λ is the wavelength, H_m is a Hermite polynomial. $\omega(q(z(j)))$ is the beam radius of the fundamental mode. $\phi_m\left(z_{(j)}\right)$ and $\phi_n\left(z_{(j)}\right)$ denote the Gouy phase shifts in the x-y and y-z planes, respectively, which is an important factor that makes the triangular cavity different from the straight cavity.

It is well known that the propagation of laser in free space can be expressed by the ABCD law [21].

$$q(z'_{(j+1)}) = \frac{Aq(z_{(j)}) + B}{Cq(z_{(j)}) + D}. \tag{3}$$

where A, B, C and D are elements describing the transmission matrix for free space propagation. The complex beam parameter is changed from $q(z_{(j)})$ to $q(z'_{(j+1)})$ after transmission or reflection. The beam radius and wave-front curvature of all modes change simultaneously when the q parameter is changed; thus the mode pattern changes in size and wave-front curvature accordingly.

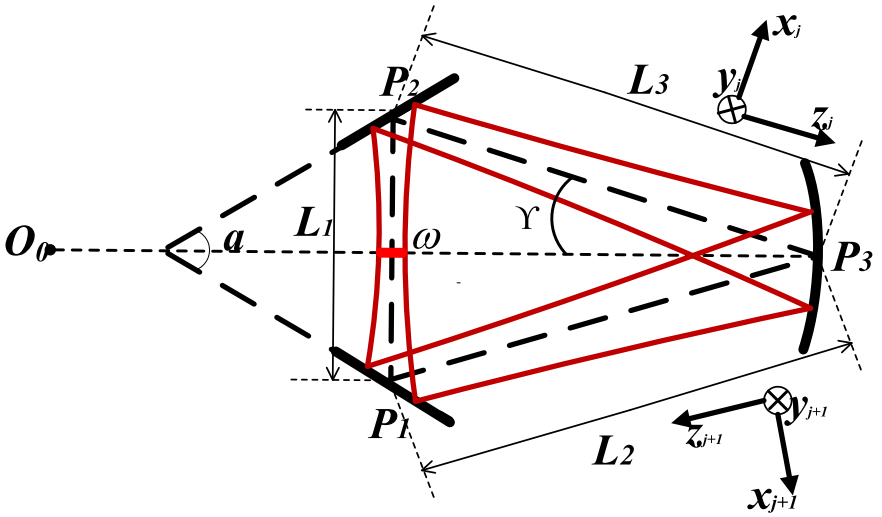

FIGURE 1. Triangular ring cavity structural parameter diagram.

The resonance characteristics of the different modes propagating in the resonator need to consider the simultaneous effects of diffraction (Gouy phase) and reflection. Firstly the Gouy phase is determined by [21]:

$$\phi_{mn}(q) = (m+n+1)\arctan\left(\frac{Req}{Imq}\right) \tag{4}$$

For reflection-induced phase shifts, the triangular cavity is different from the straight cavity, as it has no preferred transverse axis because there is no astigmatic reflector. However, for odd-plane ring cavities with spherical mirrors, it is convenient to define the transverse axes as one in the meridian plane and the other normal to that plane. The core optical element of a CRDS triangular cavity consists of two plane mirrors, P1 and P2, and a concave mirror, P3, as shown in Fig. 1. The radius of curvature of the concave mirror is R. The center of curvature of the concave mirror is O_0. Let the length of the closed optical path in the resonant cavity be $L = L_1 + L_2 + L_3$, and a be the angle between the two plane mirrors P1 and P2 cavity.

The transverse mode spacing factor of the triangular (odd) cavity is different from that of a straight cavity. Figure 1 shows the field distribution after a single reflection from a plane mirror. The y-axis direction is constant for each reflection in the triangular cavity, but the field in the x-axis direction cannot be degenerated again after three reflections. So, for resonators with an odd number of cavity mirrors, only two round-trips can be degenerated. However, this is not consistent with the theory because the destructive interference after the first round trip cannot be compensated for by the constructive interference after the second round-rip [21]. So, the most reasonable explanation is that the resonances in the x-z plane are shifted by half of the free spectral range (FSR). It should be emphasized that unlike the conventional concept of polarization, the x, y direction is the direction of distribution of the mode pattern rather than the two polarization directions of s and p. Since the resonant cavity mirror has different reflectance between different polarized light, the magnitude of the frequency shift caused is much larger than the effect brought by the frequency separation characteristics. Therefore, in the subsequent experiments, a single polarized light is adopted to analyze the frequency separation characteristics of the modal pattern, thus neglecting the effect of the polarization phase shift.

Thus when the field distribution of the modal pattern $u_{mn}(x_i, , y_i, , z_i)$ becomes $u_{mn}(-x_{(i+1)}, y_{(i+1)}, z_{(i+1)})$ after one reflection, the change produced by the reflection is expressed by the modal coefficient as:

$$a_{mn_{(j+1)}} = (-1)^m a_{mn_{(j)}} \tag{5}$$

Thus the resonance condition [22] is:

$$2\pi q = \begin{cases} kL - (m+n+1)\arctan(\sqrt{g}) & \textit{even cavity} \\ kL - (m+n+1)\arctan(\sqrt{g}) & \\ \quad -\dfrac{\pi(1-(-1)^m)}{2} & \textit{odd cavity.} \end{cases} \tag{6}$$

where $k = \omega/c$ corresponds to the wavenumber, L=$L1$+$L2$+$L3$ is the length of the straight cavity, $g = 1 - L/R$ is the cavity stability factor, and q represents the longitudinal mode number. Equation 6 shows that even though the round-trip length and phase are the same, the mode patterns in the straight and triangular cavities are different.

Thus the resonant frequency v_{mn} of each order of transverse mode in the triangular cavity can be expressed as:

$$v_{mnq} = FSR \cdot q + \frac{FSR}{\pi}(m+n+1)\arctan\left(\sqrt{1-\frac{L}{R}}\right) + \frac{FSR}{2}\frac{(1-(-1)^m)}{2} \tag{7}$$

III. TRANSMISSION AND EXCITATION OF HGS MODE IN THE ASTIGMATIC TRIANGULAR CAVITY

A. FREQUENCY-DOMAIN TRANSMISSION CHARACTERISTICS OF HGS MODE

The Hermite-Gaussian theory-based analysis of the optical resonator involves a complete spatial transverse electromagnetic mode. These eigenmodes are represented by three integer mode numbers (q, m, n), with q being the number of longitudinal mode and m and n being the numbers of transverse modes in the x- and y-axes, respectively. The transmission factor T_{mn} of the HGs mode is defined by the transmission factor of the fundamental mode, as shown in (8). T_{00} is the transmittance of the fundamental mode, S_{nm} is the suppression factor of the HGs mode [13].

$$T_{mn} = T_{00}\frac{1}{S_{mn}} \tag{8}$$

where

$$S_{mn} = \left[1 + \frac{4F^2}{\pi^2}\sin^2\left(\frac{2\pi\,\Delta\nu_{mn}}{c}L\right)\right]^{1/2}. \tag{9}$$

where F is the finesse, which is dependent on the reflectivity of the cavity mirror. c is the speed of light. Assuming that the fundamental mode resonant frequency in the cavity is the frequency of the radiation exciting the cavity, $\Delta\nu_{mn}$ is the frequency difference between the fundamental mode and any HGs mode associated with the same q, which we call the *frequency spacing factor*.

$$\Delta\nu_{mnq} = \frac{FSR}{\pi}(m+n)\arctan\left(\sqrt{1-\frac{L}{R}}\right) + \frac{FSR}{2}\frac{(1-(-1)^m)}{2}. \tag{10}$$

Combining (8) and (10) the transmission factor is given by:

$$T_{mn} = T_{00}\frac{1}{\left[\sin^2\left((m+n)\arccos\left(\sqrt{1-\frac{L}{R}}\right)\cdot\frac{4F^2}{\pi^2} + \frac{\pi(1-(-1)^m)}{4}\right)+1\right]^{1/2}} \tag{11}$$

In (11), $[\pi(1-(-1)^m)/4]$, which we call the *frequency separation factor*, corresponds to the frequency shift between modes of the same order and only occurs when the horizontal mode m is odd. Even if TEM_{11} and TEM_{20} have the same value of $(m+n)$, since they have different eigenfrequencies, they require different g-factors to resonate in the triangular cavity. Therefore, unlike the straight cavity, the first-order modes TEM_{10} and TEM_{01} also have different eigenfrequencies. Fig. 2 show that the same order mode in the triangular cavity corresponds to different g-factors. The transmission intensity is characterized by the ratio of the transmittance of the HGs modes to the fundamental mode in Fig. 2.

Although the mismatch is caused by the astigmatism of the Gaussian laser beam in the triangular cavity, Figure 3 shows that for the resonant frequencies of the astigmatic and non-astigmatic cavities of the same order modes,

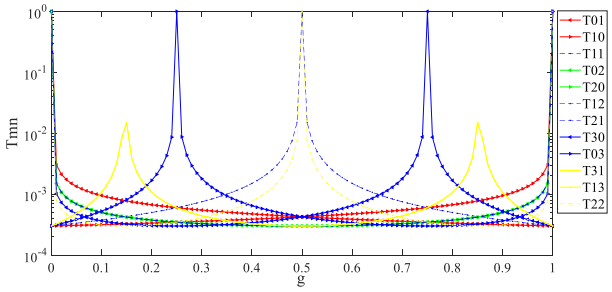

FIGURE 2. HGs modes transmittance of a Gaussian laser beam with different g-factors in a triangular ring-shaped cavity.

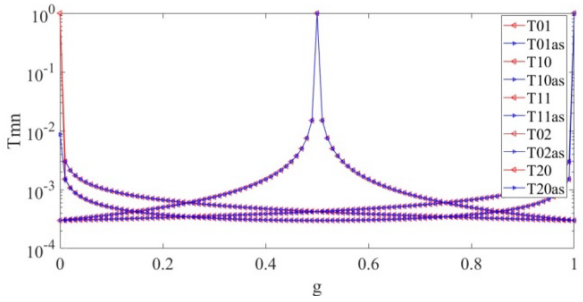

FIGURE 3. HGs modes transmittance of a Gaussian laser beam with different g-factors in a triangular ring-shaped cavity, the blue line is the astigmatic triangular cavity and the red is the non-astigmatic one.

the frequency drift due to the astigmatism factor is almost negligible.

$$T_{mn}as = T_{00}\frac{1}{\left[1+\frac{4F^2}{\pi^2}\sin^2\left(m\cdot\arccos\left(\sqrt{1-\frac{L}{R\cos\gamma}}\right)+n\cdot\arccos\left(\sqrt{1-\frac{L\cos\gamma}{R}}\right)+\frac{\pi(1-(-1)^m)}{4}\right)\right]^{1/2}} \tag{12}$$

The transmittance of the lower-order mode of HGs versus cavity radius is given in Fig. 4. The resonant frequencies of each lower-order mode at different cavity radii can be seen at the projection points in the figure. Comparing Figs 4(a) and 4(b), it can be seen that the linear Fabry-Perot resonator can only be a subset of the triangular ring cavity. As the radius of cavity curvature increases, the Gouy phase shift factor approaches 0 as g approaches 1. The frequencies of all transverse mode of the same longitudinal mode (q-identical) gradually converge. This means that most of the HGs modes will have a smaller transverse mode spacing than the fundamental mode. Thus, the fundamental mode will be transmitted together with the HGs mode. In this case, the curved mirror is close to being flat. The resonant cavity has extreme angular sensitivity. When the radius of curvature of the cavity is reduced, the transmission ratio of the HGs mode increases steeply and cannot play a role in suppressing the transmission of the HGs mode. Therefore,

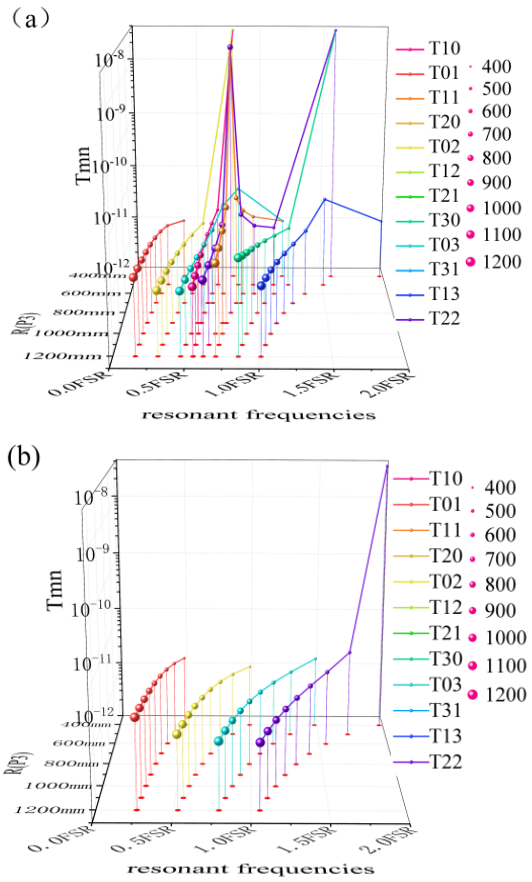

FIGURE 4. HGs mode transmittance of a Gaussian laser beam for different end-mirror radii in a (a) triangular ring-shaped cavity and (b) straight cavity.

the cavity structural parameters affect both the mounting sensitivity and transmission suppression ratio of HGs mode. The cavity structural design and experimental stages need to be considered comprehensively.

B. AMPLITUDE OF MISADJUSTED EXCITED HGS MODE

The detection efficiency of HGs depends not only on the transmission efficiency but also on the excitation intensity. Maladjustments have been considered to be the cause of excitation of the HGs mode. Maladjustment is classified as misalignment and mismatch. Figure 5 shows the schematic diagram of maladjustment of the optical path L1 between the triangular cavity reflector P1 and P2. Because the misalignment of the light source and the cavity is only in the L1 optical path, the expression in Figure 5 is the misalignment and mismatch of the L1 optical path. Misalignment is the non-coincidence of the optical axes of the injected beam and the beam in the cavity. Figure 5 (a) shows a mismatch in the beam waist size, while Fig. 5 (b) shows a shift in the beam waist in the case of the same optical axis. The misalignment error can be expressed in terms of ε_v, α_v with v representing the x or y factor. The misalignment is caused by the transverse shift (ε_x, ε_y) and tilt (α_x, α_y) of the optical axis between the

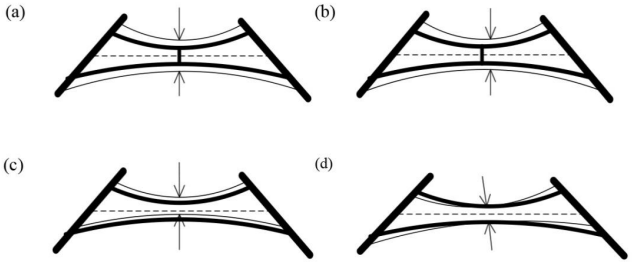

FIGURE 5. Diagram of misalignment and mismatch in a triangular cavity. The thick line represents the cavity beam and beam waist (ω), and the thin line and arrow represent the incident beam and beam waist (ω'). (a, b) Two cases of a mismatched beam, and (c, d) two cases of a misaligned beam.

injected beam and the intracavity beam, as shown in Figs. 5 (c)–(d), respectively.

For the four maladjustment cases shown in Fig. 5, the Hermite-Gaussian function can be separated as the product of two functions. The two functions are independent of each other. In the next analysis, we will address the x-variable. The y-variable is ignored because it is equivalent to x. For the four maladjustment cases shown in Fig. 5, Sayeh provided misalignment and mismatch parameters [16], where $\xi_v = (\varepsilon_v - q_{Lv}\alpha_v)\,\omega$ is the misalignment parameter, where ω represents the size of the cavity Gaussian beam waist and $o_v = \left[(q_v - q_{Lv})/(q_v + q_{Lv})\right]^{1/2}$ is the mismatch parameter, where q_{Lv} and q_v are the q-parameters of the beam injected by the external source laser and the intracavity beam, respectively. The proposed parameter quantifies the effect of the misalignment mismatch. The power transfer from the fundamental mode to the HGs mode caused by the misadjustment can be expressed as [16]:

$$A_\mu/A_0 = \left(o_x^\mu/\sqrt{2^\mu \mu!}\right) H_\mu\left[\xi_x\left(1+o_x^2\right)/\sqrt{2}\,o_x\right]. \quad (13)$$

here μ (which can be m or n) is the order of the transverse mode. There are two special cases when $o_v \to 0$ (matching is complete). Using a Hermite polynomial to make the approximation $H_\mu(x) \approx (2v)^\mu$, then:

$$I_\mu = I_0 \cdot \left(2\pi e^{-2}\right)^{-1/2} (\varepsilon_v - q_{Lv}\alpha_v)^2 \quad (14)$$

When $\xi_v \to 0$ (perfect alignment), Stirling's approximation is made for the equation: when μ is odd $H_\mu(x) \approx 0$, and when μ is even, $H_\mu(x) \approx (-1)^{\mu/2}\,\mu!/(\mu/2)!$, then (13) can be simplified to:

$$\begin{cases} I_{2\mu} = I_0\left(-o_x^2\right)^{2\mu}/(\pi\mu)^{1/2} \\ I_{2\mu+1}/I_0 = 0 \end{cases} \quad (15)$$

From (13), it can be seen that as the transverse mode increases from first-order to higher-order, the excitation of the higher-order mode decreases sharply; hence, it is apparent that the maladjustment mainly excites the lower-order mode. Taking the first- and second-order modes as an example, comparing (14) with (15) within the allowable range of

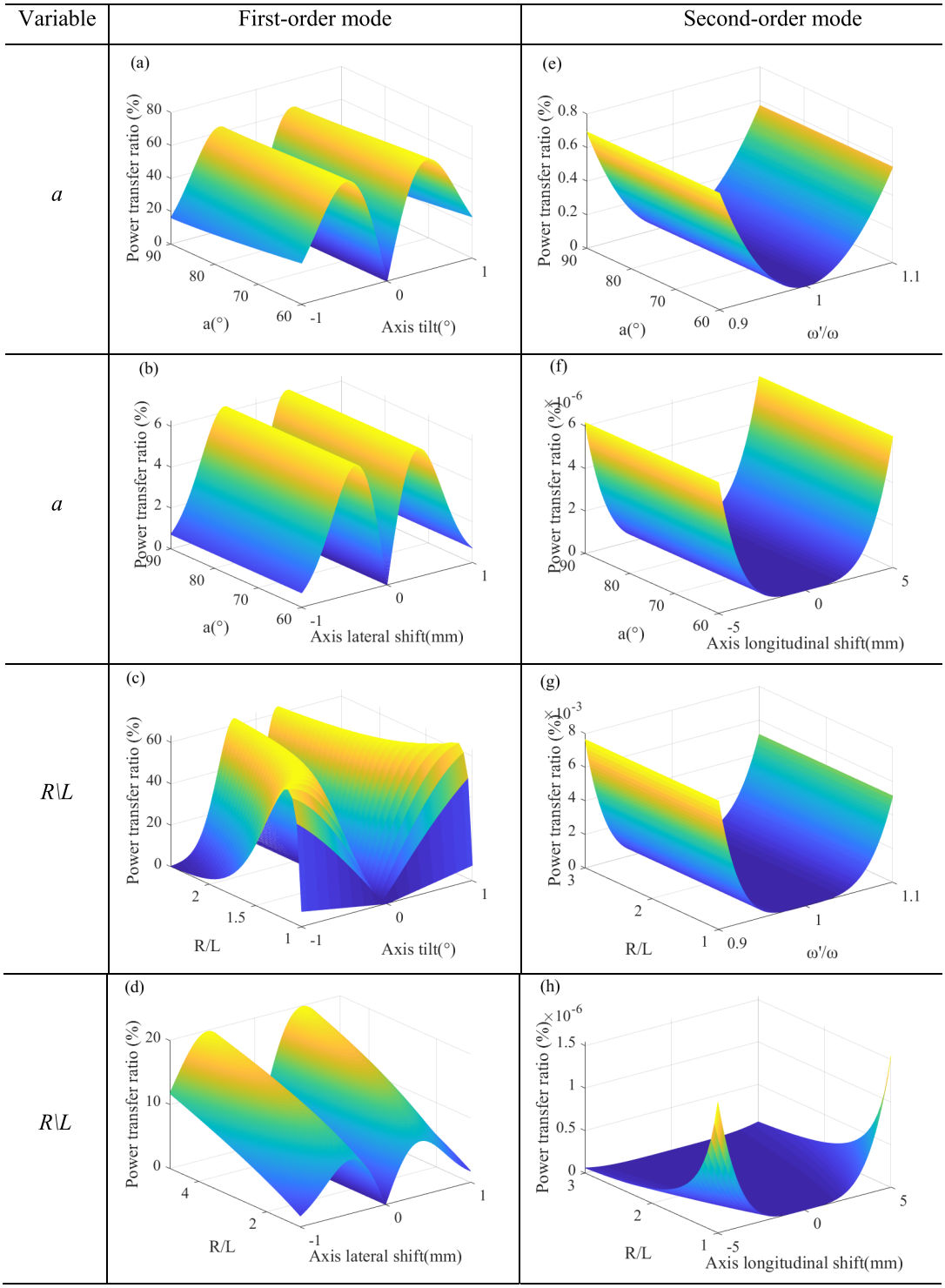

FIGURE 6. Power transfer in misalignment mismatch systems with low-order mode of Gaussian laser beams. (a-d) are the first-order mode for misaligned excitation, and (e-h) are the second-order mode for mismatch excitation. When only misalignment exists, the excitation intensity of the first-order mode varies with (a) α_v and (b) ε_v for a fixed end-mirror radius R/L and a varying angle a. The excitation intensity of the first-order mode varies with (c) α_v and (d) ε_v when a = 88.56° and R/L varies. When there is only a mismatch, the excitation intensity of the second-order mode varies with (e) ω'/ω and (f) axis longitudinal shift when R/L is fixed and a is varies. The excitation intensity of the second-order mode varies with (g) ω'/ω and (h) axis longitudinal shift when a = 88.56° and R/L varies.

mounting error shows that the excitation of the first-order mode is much stronger than that of the second-order mode. As the misalignment and mismatch increase, the first-order modes manifest non-monotonicity, while the second-order modes are monotonically increasing, and the misalignment error excitation of the second-order modes is 10^7 orders of

magnitude less than the excitation of the first-order modes. Excitation of the first-order mode is preferred, and when caused by axis tilt, it is stronger than that caused by the axis traverse. Comparing Figs. 6(a, c) with 6(b, d), we can see that the extreme value of the first-order mode due to axis tilt is greater than that due to axis traverse. The excitation of the first-order mode by misalignment shows a tendency to be enhanced and then weakened as the error increases. As the error gradually increases, the first-order mode excitation is enhanced. However, when the error increases to a certain degree, the first-order mode of the fundamental mode will be weakened at the same time, and the higher-order mode shows a faster ring-down rate because its area is larger than that of the fundamental mode.

Excitation of the low-order mode is not only related to the amount of maladjustment but also cavity structure variation. Figures 6(a) and (b) illustrate that the variation in cavity angle a does not affect the mounting sensitivity. However, the radius R of the curved mirror P3 directly affects the stability of the cavity. When the R/L ratio is 1 (g-factor = 0), excitation of the first-order mode is significantly reduced at the same error level. The triangular cavity is more sensitive to error as R/L increases at the same error level and the cavity becomes almost unstable as the g-factor approaches 1.

The transmission characteristics and amplitude excitation trends of the HGs mode for each structural parameter of the triangular cavity are discussed in this section. From the analysis, it is concluded that not only the effect of maladjustment needs to be considered to give higher priority to lower-order mode. Also, to avoid simultaneous transmission of fundamental and HGs mode, the effect of transverse mode spacing between each order of HGs modes should be considered. This provides the basis for the selection of cavity structural parameters. The experiments, described next, verify the resonant frequency separation characteristics of low- and high-order HGs modes in a high-finesse triangular cavity.

IV. EXPERIMENT

To verify the frequency domain distribution and transmission characteristics of each order of HGs mode, a physical cavity was not used in the first stage of alignment experiments, so that the cavity structural parameters could be changed by moving the cavity mirror position. The transmission characteristics of each order of mode within one FSR of the cavity were first scanned to obtain mode scan maps. It was found that the astigmatism of the triangular cavity exacerbated the excess excitation of the second-order mode, and the relationship between the first-order mode and the amount of misalignment was observed.

To identify the HGs mode, the cavity mode needed to be scanned. After mode identification, the excitation properties of the first-order mode were explored by introducing misalignment. Figure 7 shows the apparatus used to demonstrate the HGs mode excitation and mode-scan experiments. The entire system was mounted on a single vibration isolation platform. The center of rotation of a six-dimensional precision adjustment frame (APFP-XYZTθ) was on the same optical axis as the center of the three cavity mirrors. The cavity structure could be changed by moving the position of the frame. The triangular cavity consisted of two planar mirrors and one curved mirror. The length of the round-trip was L = 420 mm, the reflectivity at 1653 nm was 99.97%, the radius of the curved mirror was 1 m, the angle between the two planar mirrors was 88.542°, and the free spectral range was 714.3 MHz. Therefore, the finesse of the cavity is about 10000 according to the finesse formula of the triangular cavity. The curved mirror was mounted on a piezoelectric transducer (PZT; P-841.10) to scan the cavity length. Alignment of the intracavity beam and the introduction of misalignment were accomplished by adjusting two planar mirrors, M1 and M2, which could be tilted at an angle controlled by the PZT. The light source was a single-mode fiber-distributed feedback laser (DFB; EP1653-DM-B) with a rated power of 3 mW and a linewidth of 2 MHz. A telescope-like matching lens with a column lens set was placed behind the laser to adjust the beam waist radius. The existence of spherical aberration in the collimation process is also included in the discussion of the mismatch case. The matching mirror was followed by a polarizing beam splitter, where the p-polarized light was incident into the cavity to eliminate the effect of the different resonant frequencies of the s- and p-polarized light on the establishment of resonance in the cavity. The cavity outgoing light passed through a focusing lens into an InGaAs switchable gain detector (Thorlab PDA10CS2), and a mixed-signal oscilloscope (MSO; MSO6104A) recorded the avalanche photodiode detector (APD) signal. A computer controlled the experiments and recorded the data.

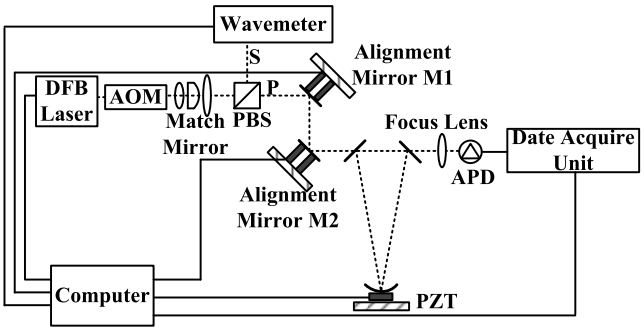

FIGURE 7. Structural diagram of the cavity alignment experimental setup.

(1) HGs mode identification was achieved by using the PZT to change the cavity length behind the curved mirror for mode scanning. The mode scan experiment does not require the PDH method typically used in CRDS measurements, and the frequency of the source is precisely controlled by a wavelength meter that scans the triangular cavity for HGs modes within a free spectral range of 714.3 MHz. The identification of HGs mode was achieved by sweeping the frequency for mode scanning. The sampling rate of the instrument was determined by the response rate of the detector. Since the detector had an adjustable gain, its bandwidth varied with the gain size. The bandwidth was 300 kHz when

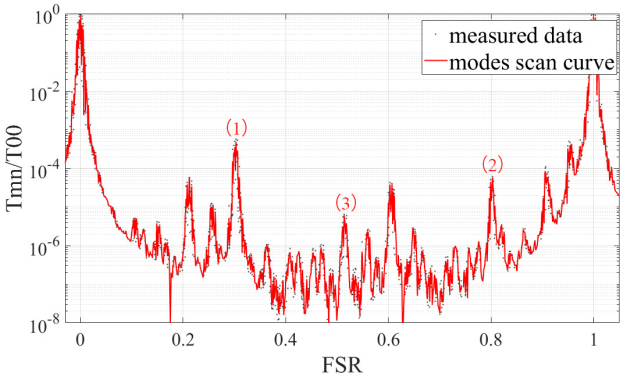

FIGURE 8. Mode scanning in a high-finesse triangular ring cavity.

a 30 dB gear was used, and the fastest response time was 1.2 μs. The oscilloscope set the sampling rate shot to 500k samples/s with the detector. A ramped signal was applied to the PZT of the resonant cavity's curved mirror P3, so that the cavity length was scanned in the range of 2.5 FSR, and an FSR scan rate of 80 FSR/S was obtained. Approximately 5000 data points were collected within each FSR to describe the mode information over a free spectral range. The piezoelectric element needed to be calibrated before the experiment to eliminate hysteresis. Figure 8 shows a curve of the HGs mode fit within one FSR range for a certain rough alignment case.

The fitted results were compared with the model given in (11) to determine the position of each HGs mode resonance peak. Since the high-finesse cavity provided stronger suppression of the transmission ratio of the HGs mode, the combination of the excitation characteristics of the first-order mode in (14) determined a transmission ratio of $> 10^{-4}$ for the first-order mode. The fitted results show that the TEM_{01}((1) in Figure 8) mode had stronger excitation than TEM_{10}((2) in Figure 8), indicating that the misalignment was mainly in the y-z plane. The analysis of the second-order mode shows that TEM_{20} and TEM_{02}((3) in Figure 8) had stronger excitations than the theoretical values. By designing the radius of the beam waist in the meridian plane and sagittal surface separately, the excitation of the second-order mode was significantly reduced by adding a column lens to the matched mirror. Since the mismatch was the main cause of the second-order mode excitation, it can be seen that the mismatch phenomenon in the triangular cavity was, to some extent, related to astigmatism.

(2) Mode scanning experiments can determine the location of the resonance peak of the first-order mode. Control of the misalignment error was accomplished by two alignment mirrors, M1 and M2, from which the relationship between misalignment and first-order mode excitation was measured, while the angular tilt of the alignment mirrors was controlled by the PZT. The pure angular tilt between the incident beam and cavity beam was generated by M2, which was close to the input mirror. Optical axis translation was achieved by the combined motion of Ml and M2. To prevent some of the light

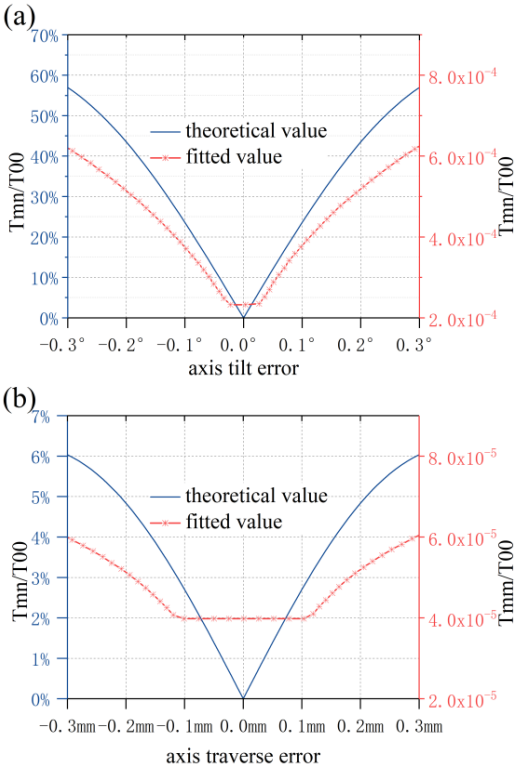

FIGURE 9. L = 420 mm, R = 1000 mm, a = 88.56°. First-order transverse mode power transfer ratio variation with (a) axis tilt error and (b) axis traverse error.

from exceeding the detection range when the tilt angle was too large, the tilt angle (α_v) range was $\pm$ 0.3° and the axis translation (ε_v) range was $\pm$ 0.3 mm [20]. The error was reduced by averaging the results of multiple measurements under the same misalignment condition over several sweeps of frequency measurements.

Figures 9(a)–(b) show the excitation of the first-order mode in the two cases of axial tilt and axial transverse shift, respectively. The blue line is the theoretical value obtained from (14) and the red line represents the curve fitted to the measured TEM_{10} values in the x-z plane of incidence, with the same trend for TEM_{01} in the y-z plane. Comparing Figs. 9(a) and (b), it can be seen that the axial tilt error produces a stronger first-order mode excitation, which is the same conclusion as made in Section 3, while the high-finesse cavity provides an additional suppression factor for the HGs mode. The fitted curves are limited by the detector's sensitivity when the error is small, and cannot produce a linear change for tilt errors less than $\pm$ 0.02° with an axial shift error of $\pm$ 0.11 mm. The curves fitted to the measured data exhibit lower excitation enhancement rates than the theoretical values, and the rate of increase slows down further as the error increases, because the beam cannot enter the range of the detector as the tilt and axis traverse increase.

This part of the experiment verifies the frequency separation characteristics of the first-order mode. The alignment experiments show that although the high-finesse cavity enhances the suppression of HGs modes, it still exhibits a

relationship between the first-order mode and the misaligned quantities. Anderson's method proposes that the alignment of both ε_v and α_v can be guided by the amplitude and phase of the first-order mode, respectively [17]. However, it is more difficult to obtain accurate information on the phase sidebands for a low-power multimode system like CRDS. The quadrant detector is unable to detect CRDS systems with a cavity finesse of 10,000 due to the limitation of sensitivity, Therefore, the method of Anderson *et al.* cannot be applied to CRDS systems with extremely low transmission energy. Since ε_v and α_v are orthogonal, the axial shift error and tilt error have different magnitudes of influence on the first-order mode, and the two errors can be aligned separately in the initial stage of mounting. Meanwhile, the triangular cavity TEM_{10} and TEM_{01} transverse mode spacing do not overlap, allowing misalignment information in the x-z and y-z planes to be obtained.

V. CONCLUSION

In this paper, we investigated the mechanisms of the different effects of the HGs mode in first and second-order modes on the mounting alignment of CRDS systems. Based on Hermit-Gaussian theory, the resonant frequency separation characteristics of the same-order HGs mode in a high-finesse triangular cavity were analyzed. These characteristics are the essential differences between triangular and straight cavities. To study the excitation of HGs modes, first- and second-order modes amplitudes were analyzed in different triangular cavity structures. The resonant frequency separation characteristics and amplitude excitation trends of the triangular cavity HGs mode were verified in the mounting alignment stage. The separation characteristics of the HGs mode can guide the alignment of two orthogonal planes separately. However, high sensitivity detectors are still necessary in ring-down experiments due to the transmission suppression of high finesse cavities. In this paper, the resonant frequency separation characteristics of the same-order Hermite-Gaussian mode in the astigmatic triangular cavity are proposed, which further improves the HGs mode theory. It is also demonstrated that the CRDS triangular cavity system not only has the advantages of eliminating optical feedback, but also can further improve the mounting accuracy in the static mounting alignment stage (before the ring-down measurement).

REFERENCES

[1] G. Berden, R. Peeters, and G. Meijer, "Cavity ring-down spectroscopy: Experimental schemes and applications," *Int. Rev. Phys. Chem.*, vol. 19, no. 4, pp. 565–607, Nov. 2010.

[2] G. N. Rao and A. Karpf, "High sensitivity detection of NO_2 employing cavity ringdown spectroscopy and an external cavity continuously tunable quantum cascade laser," *Appl. Opt.*, vol. 49, no. 26, pp. 4906–4914, Sep. 2010.

[3] G. Genoud, M. Vainio, H. Phillips, J. Dean, and M. Merimaa, "Radiocarbon dioxide detection based on cavity ring-down spectroscopy and a quantum cascade laser," *Opt. Lett.*, vol. 40, no. 7, pp. 1342–1345, Apr. 2015.

[4] A. Bicer, J. Bounds, F. Zhu, A. A. Kolomenskii, S. Tzortzakis, and H. A. Schuessler, "Cavity ring-down spectroscopy for the isotope ratio measurement of methane in ambient air with DFB diode laser near 1.65 μm," in *Proc. Conf. Lasers Electro-Opt. Eur., Eur. Quantum Electron. Conf. (CLEO/Europe-EQEC)*, Jun. 2017, p. 39.

[5] W. Chen, K. Roslund, C. L. Fogarty, P. J. Pussinen, L. Halonen, P.-H. Groop, M. Metsälä, and M. Lehto, "Detection of hydrogen cyanide from oral anaerobes by cavity ring down spectroscopy," *Sci. Rep.*, vol. 6, no. 1, p. 22577, Mar. 2016.

[6] C. Wang, A. Mbi, and M. Shepherd, "A study on breath acetone in diabetic patients using a cavity ringdown breath analyzer: Exploring correlations of breath acetone with blood glucose and glycohemoglobin A1C," *IEEE Sensors J.*, vol. 10, no. 1, pp. 54–63, Jan. 2010.

[7] P. Jacquet, A. Pailloux, G. Aoust, J.-P. Jeannot, and D. Doizi, "Cavity ring-down spectroscopy for gaseous fission products trace measurements in sodium fast reactors," in *Proc. 3rd Int. Conf. Advancements Nucl. Instrum., Meas. Methods their Appl. (ANIMMA)*, Jun. 2013, pp. 1–5.

[8] T. K. Boyson, D. R. Rittman, T. G. Spence, K. P. Kirkbride, D. S. Moore, and C. C. Harb, "Rapid, wideband cavity ringdown spectroscopy for the detection of explosives," in *Proc. CLEO*, 2014, pp. 1–2.

[9] A. Maity, S. Maithani, and M. Pradhan, "Cavity ring-down spectroscopy: Recent technological advancements, techniques, and applications," *Anal. Chem.*, vol. 93, no. 1, pp. 388–416, Jan. 2021.

[10] J. Yuan, X. Long, B. Zhang, F. Wang, and H. Zhao, "Optical axis perturbation in folded planar ring resonators," *Appl. Opt.*, vol. 46, no. 25, pp. 6314–6322, Aug. 2007.

[11] J. Yuan, M. Chen, Y. Li, Z. Tan, and Z. Wang, "Reanalysis of generalized sensitivity factors for optical-axis perturbation in nonplanar ring resonators," *Opt. Exp.*, vol. 21, no. 2, pp. 2297–2306, Jan. 2013.

[12] C. Li-Hong, Y. Chang-Xiang, Z. Wei-Ning, Z. Xin-Jie, and H. Chun-Hui, "Analysis of the positional accuracy of the self-conjugate ray in a misalignment multiple-mirror optical ring cavity," *Acta Phys. Sinica*, vol. 64, no. 22, 2015, Art. no. 224210.

[13] J. W. Hahn, Y. S. Yoo, J. Y. Lee, J. W. Kim, and H. W. Lee, "Cavity ringdown spectroscopy with a continuous-wave laser: Calculation of coupling efficiency and a new spectrometer design," *Appl. Opt.*, vol. 38, no. 9, pp. 1859–1866, Mar. 1999.

[14] S. Solimeno and A. Cutolo, "Coupling coefficients of mismatched and misaligned Gauss–Hermite and Gauss–Laguerre beams," *Appl. Opt.*, vol. 11, no. 3, pp. 141–143, Mar. 1986.

[15] W. Qiao, Z. Xiaojun, L. Zongsen, W. Yonggang, S. Liqun, and N. Hanben, "Simple method of optical ring cavity design and its applications," *Opt. Exp.*, vol. 22, no. 12, pp. 14782–14791, Jun. 2014.

[16] M. R. Sayeh, H. R. Bilger, and T. Habib, "Optical resonator with an external source: Excitation of the Hermite-Gaussian modes," *Appl. Opt.*, vol. 24, no. 22, pp. 3756–3761, Nov. 1985.

[17] D. Z. Anderson, "Alignment of resonant optical cavities," *Appl. Opt.*, vol. 23, no. 17, pp. 2944–2949, Sep. 1984.

[18] N. M. Sampas and D. Z. Anderson, "Stabilization of laser beam alignment to an optical resonator by heterodyne detection of off-axis modes," *Appl. Opt.*, vol. 29, no. 3, pp. 394–403, Jan. 1990.

[19] T. Skettrup, T. Meelby, K. Færch, S. L. Frederiksen, and C. Pedersen, "Triangular laser resonators with astigmatic compensation," *Appl. Opt.*, vol. 39, no. 24, pp. 4306–4312, Aug. 2000.

[20] S. Song, C. Hu, and C. Yan, "Optical axis maladjustment sensitivity in a triangular ring resonator," *Appl. Opt.*, vol. 58, no. 1, pp. 29–36, Jan. 2019.

[21] M. Möller, L. M. Hoffer, G. L. Lippi, T. Ackemann, A. Gahl, and W. Lange, "Fabry–Pérot and ring cavity configurations and transverse optical patterns," *J. Modern Opt.*, vol. 45, no. 9, pp. 1913–1926, Sep. 1998.

[22] C. Mathis, C. Taggiasco, L. Bertarelli, I. Boscolo, and J. R. Tredicce, "Resonances and instabilities in a bidirectional ring laser," *Phys. D, Nonlinear Phenomena*, vol. 96, nos. 1–4, pp. 242–250, Sep. 1996.

YIJIE REN was born in Changzhi, Shanxi, China, in 1994. He received the B.S. degree in measurement and control technology and instrument from the Changchun University of Science and Technology, China, in 2018. He is currently pursuing the Ph.D. degree in optical engineering with the Changchun Institute of Optics, Fine Mechanics and Physics, Chinese Academy of Sciences, Changchun, China. His current research interests include cavity ring-down spectroscopy and trace gas detection.

CHANGXIANG YAN was born in Honghu, Hubei, China, in 1973. He received the M.S. degree in engineering from Zhejiang University, Zhejiang, China, in 1998, and the Ph.D. degree from the Changchun Institute of Optics, Fine Mechanics and Physics, Chinese Academy of Sciences, Changchun, China, in 2001.

Since 2010, he has been the Director with the Space Optics Laboratory of Changchun Institute of Optics, Fine Mechanics and Physics, Chinese Academy of Sciences. His research interests include opto-mechatronics technology for space optical remote sensing instruments, multispectral and hyperspectral spatial remote sensing imaging, cavity ring-down spectroscopy, polarization detection, and space surveillance.

CONGJUN WU was born in Ankang, Xi'an, China, in 1986. He received the Ph.D. degree from the Changchun Institute of Optics, Fine Mechanics and Physics, Chinese Academy of Sciences, Changchun, China, in 2014. His current research interests include optical design and optical system image quality research.

SHAOMAN SONG was born in Yuncheng, Shandong, China, in 1988. He received the B.S. degree from Shandong University, Shandong, in 2014, and the Ph.D. degree from the Changchun Institute of Optics, Fine Mechanics and Physics, Chinese Academy of Sciences, Changchun, China, in 2019. His current research interests include cavity ring-down spectroscopy and optical design research.

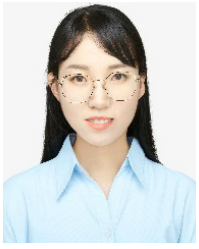

JING YUAN was born in Changchun, Jilin, China, in 1993. She received the B.S. degree in optical information science and technology from Jilin University, China, in 2016, and the Ph.D. degree from the Changchun Institute of Optics, Fine Mechanics and Physics, Chinese Academy of Sciences, Changchun, China, in 2021. Her current research interests include application of spectra, hyper-spectral remote sensing, and application of remote sensing in soil.